

Stereo Event-based Visual-Inertial Odometry

Kunfeng Wang, Kaichun Zhao

Abstract— Event-based cameras are new type vision sensors whose pixels work independently and respond asynchronously to brightness change with microsecond resolution, instead of provide standard intensity frames. Compared with traditional cameras, event cameras have low latency, no motion blur, and high dynamic range (HDR), which provide possibilities for robots to deal with some challenging scenes. We propose a visual-inertial odometry method for stereo event-cameras based on Kalman filtering. The visual module updates the camera pose relies on the edge alignment of a semi-dense 3D map to a 2D image, and the IMU module updates pose by midpoint method. We evaluate our method on public datasets in natural scenes with general 6-DoF motion and compare the results against ground truth. We show that the proposed pipeline provides improved accuracy over the result of a state-of-the-art visual odometry method for stereo event-cameras, while running in real-time on a standard CPU. To the best of our knowledge, this is the first published visual-inertial odometry algorithm for stereo event-cameras.

MULTIMEDIA MATERIAL

Video: <https://youtu.be/IclaeypKIPc>

Code: <https://github.com/WKunFeng/SEVIO>

I. INTRODUCTION

Simultaneous localization and mapping (SLAM) has important applications in many emerging technologies such as robotics, intelligent transportation, and augmented/virtual reality (AR/VR). There are already a lot of works on slam based on traditional cameras [1], [2]. However, traditional cameras may fail in some challenging situations such as high-speed motions or high dynamic range scenes.

Event-based cameras are bio-inspired vision sensors work very different from traditional cameras which report the pixel-wise intensity changes asynchronously at the time they occur, called “events” [3], [4], where each event consists of its space-time coordinates and the sign of the brightness change (e.g., 0 or 1). Event cameras have different types of sensors, such as the Dynamic Vision Sensor (DVS) [3], the DAVIS [5] or the ATIS [6]. Thus, they don’t output an intensity image at a fixed rate but a stream of asynchronously events at microsecond resolution. Event cameras have numerous advantages over traditional cameras, such as a latency of microseconds, low power consumption, and a very high dynamic range (e.g., 140 dB compared to 60 dB of standard cameras). With microsecond resolution, event cameras can work at high-speed motions, which would cause severe motion blur on traditional cameras. High dynamic range allow

Kunfeng Wang and Kaichun Zhao are with the Department of Precision Instrument at the Tsinghua University, Beijing, China. (E-mail: wkf18@mails.tsinghua.edu.cn, kaichunz@tsinghua.edu.cn).

Zheng You (Corresponding author) is with the Department of Precision Instrument at the Tsinghua University, Beijing, China. (E-mail: yz-dpi@mail.tsinghua.edu.cn).

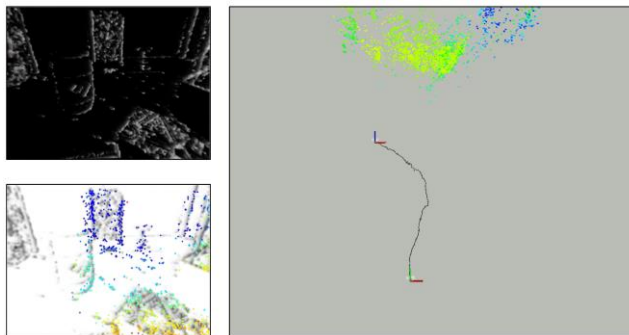


Figure 1. Top left: time surface. Bottom left: warped depth map overlaid on the time surface negative at the current time. Right: pose estimation

them to be used on broad illumination scenes. Thus, event cameras have the potential to tackle challenging scenarios in robotics.

The main challenge is how to unlock the potential of event cameras for SLAM and other vision tasks [4]. This is due to the fact that the output of event cameras is different from that of traditional cameras, so that frame-based vision algorithms designed for image sequences are not directly applicable to event data. Thus, we need new methods to process the data from these novel cameras. There are already some works for event cameras, such as feature tracking [7], [8], [9], 3D orientation estimation [10], [11], [12], [13], and simultaneous localization and mapping (SLAM) [14], [15], [16].

In this paper we propose a stereo visual-inertial odometry (VIO) for event cameras in natural scenes and arbitrary 6-DoF motion. Our pipeline has three parallel threads, tracking, mapping, and IMU integral. For the visual module, we use the strategy of ESVO [16]. IMU integral using the median method, and fusion strategy is EKF. Our contributions are as follows:

- A novel visual-inertial odometry for stereo event cameras. To the best of our knowledge, this is the first published visual-inertial odometry algorithm for stereo event cameras.
- When there are few or no events, for example, the movement of event cameras is slow or stationary. Our system can temporarily use pure inertial data, increasing the robustness of the system.
- A quantitative evaluation of our pipeline compared to the ESVO on the public event camera dataset, demonstrating that the system is more accurate. The code has been open sourced.

Pure vision-based SLAM/VO algorithms generally are less accurate and lack robustness in some challenging conditions, and fusion with additional sensors such as an Inertial Measurement Unit (IMU) is a common solution.

II. RELATED WORK

In the past few years, many works have been proposed to use event cameras for ego-motion estimation. Here we review some of those literature [4].

A. Event-based Depth Estimation

a) monocular: Depth estimation with a single event camera has been shown in [17], [18], [19]. It is a significantly different problem from previous ones because it is difficult to match events across time. These methods produce a semi-dense 3D reconstruction (i.e., 3D edge map) of the scene with the information of the camera motion over time. Thus, they do not pursue instantaneous depth estimation, but rather depth estimation for SLAM/VO.

b) stereo: Most works on depth estimation with event cameras using events on a very short time (ideally on a per-event basis) from two or more synchronized cameras that are rigidly attached. The events from different camera image planes share a common clock. Then, following the classical two-step stereo paradigm, first match the events across image planes and then triangulate the location of the 3D point [20]. The problem is finding correspondences between events. Events are matched (i) using traditional stereo metrics (e.g., normalized cross-correlation) on event frames [21], [22] or time surface [23], [24] or (ii) by exploiting simultaneity and temporal correlations of the events across sensors [23], [25], [26]. Most of these methods are demonstrated in scenes with static cameras and few moving objects, so that correspondences are easy to find.

B. Event-based 3-DOF Estimation

3-DOF estimation include pure rotation [10], [11], [12], [13] and planer motions [27].

Cook et al. [10] proposed an algorithm to jointly estimate ego-motion, image intensity and optical flow from events with an interacting network. However, it only applies to pure rotational motion. The filter-based approach in [11] used probabilistic filters in parallel to track the 3D orientation of a rotating event camera and create high-resolution panoramas of natural scenes. Rotational motion estimation was also presented in [12], where camera tracking was performed by minimization of a photometric error at the event locations given a probabilistic edge map. A motion-compensation optimization framework was introduced in [13] to estimate the angular velocity of the camera rather than its absolute rotation. All of the above works are limited to rotation estimation, not translation.

An event-based 2D SLAM system was presented in [27], and it was restricted to planar motion and high-contrast scenes. This method used a particle filter for tracking, with the event likelihood function inversely related to the reprojection error of the event with respect to the map.

C. Event-based VO

Solutions to the problem of event-based 3D SLAM for 6-DOF motions and natural scenes, with pure event-cameras, have been proposed [16], [18], [28].

a) monocular: The approach in [18] extends [11] and consists of three interleaved probabilistic filters to perform pose tracking as well as depth and intensity estimation. However, it is computationally intensive, requiring a GPU for real-time operation. In contrast, the semi-dense approach in [28] shows that intensity reconstruction is not needed for depth estimation or pose tracking. The approach performs space sweeping for 3D reconstruction [17] and edge-map alignment (non-linear optimization with few events per frame) for pose tracking. The resulting SLAM system runs in real-time on a CPU.

b) stereo: The approach proposed in [16] tackle the problem of stereo visual odometry with event cameras in natural scenes and arbitrary 6-DoF motion in real time with a standard CPU. It reconstructs a semi-dense 3D map following two steps: (i) computing depth estimates of events and (ii) fusing such depth estimates into an accurate and populated depth map [24].

D. Event-based VIO

To improve the accuracy and robustness of visual odometry, combining with other sensors is a common option, especially inertial measurement unit (IMU).

[29] tracked features using [8], and combined them with IMU data by a way of Kalman filter. [30] proposed to synthesize motion-compensated event images from spatio-temporal windows of events and then detect-and-track features. Feature tracks were fused with inertial data by means of keyframe-based nonlinear optimization to recover the camera trajectory and a sparse map of 3D landmarks. As opposed to the above-mentioned feature-based methods, the work in [23] optimizes a combined objective with inertial- and event-reprojection error terms over a segment of the camera trajectory, in the style of visual-inertial bundle adjustment.

III. STEREO EVENT-BASED VISUAL-INERTIAL ODOMETRY

This section presents the details of stereo event-based visual-inertial odometry. We start with an overview of the entire pipeline. Then, we introduce how to process event data so that we can use its information efficiently. After that, we give the details of visual model and IMU integral model. At least, we present how to fuse information from different sensors with EKF.

A. Framework overview

A flowchart of our proposed pipeline detailing all steps is illustrated in Figure 2. Let us briefly introduce the functionality of each module and explain how they work. First of all, the event processing module translate event stream to time-surface image, which will be used by visual modules (Section III-B). Secondly, after an initialization phase, the tracking thread of visual module continuously estimates the pose of the left event camera by efficient 3D-2D edge alignment. The mapping thread of visual module uses the events, time surfaces and pose estimates to update a local map (semi-dense depth map), which is used by the tracking

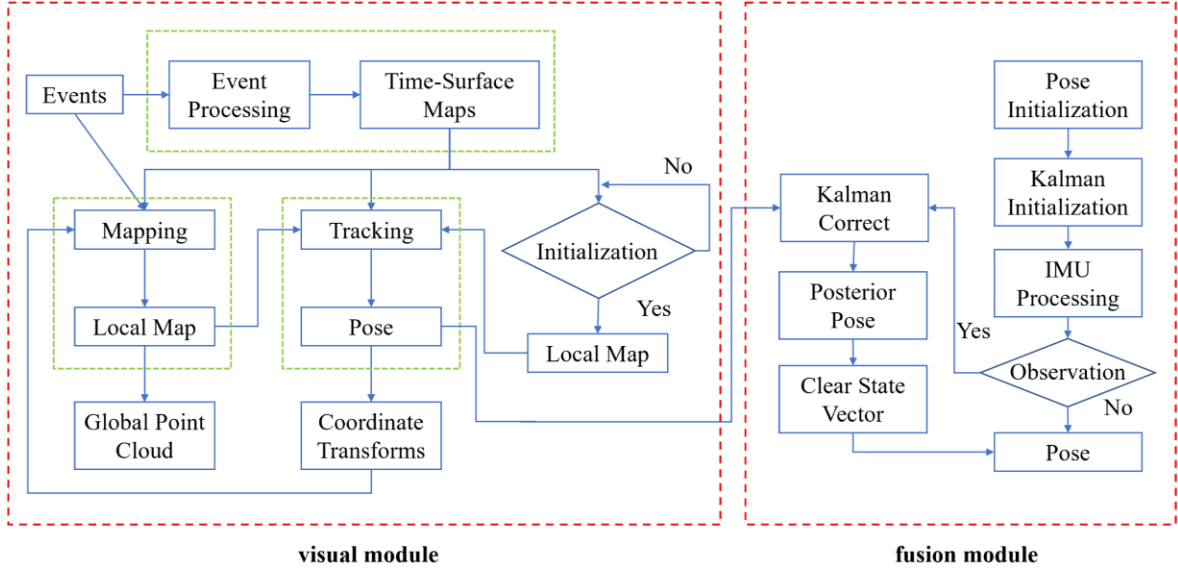


Figure 2. Overview of our proposed stereo event-based visual-inertial odometry

thread (Section III-C). At the same time, IMU integral module continues to integrate. When the mapping thread is working, EKF module receives an observation and performs a state update (Section III-D). Then, mapping module uses the fused pose to refresh local map.

Initialization: Visual module provides a coarse initial map by a stereo method (a modified SGM method [32]). The IMU module assumes that the initial state of the system is static [33], [34], using the first 1-2s (depending on dataset) of IMU data to estimate the gravity direction and the biases of the gyroscope and accelerometer.

B. Event representation (Time Surface)

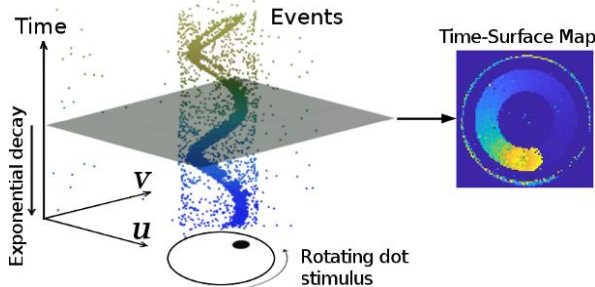


Figure 3. Event Representation. Left: Output of an event camera. Right: Time-surface map. Figure adapted from [35]

The output of an event camera is a stream of asynchronous events. Each event can be described as $e_k = (u_k, v_k, t_k, p_k)$, consists of pixel coordinate $(u_k, v_k)^T$ where intensity change of predefined size happened, timestamp t_k , and polarity p_k ($\{-1, 1\}$ or $\{0, 1\}$) of the change.

Generally, we do not process events asynchronously at the very high rate they occur, but use an alternative representation called Time Surface (Fig 3-right). A time surface (TS) is a 2D image where each pixel stores a single time value (e.g., the timestamp of the last event at that pixel [36] [37]), so that

events are converted into an image whose “intensity” is a function of the motion history at that coordinate, and larger values means closer motion history. The value at each pixel coordinate $x = (u, v)^T$ is defined by

$$\mathcal{T}(x, t) \doteq \exp\left(-\frac{t - t_{last}(x)}{\eta}\right) \quad (1)$$

where t is an arbitrary time ($t > t_{last}(x)$), and $t_{last}(x)$ is the timestamp of the last event occurring at x . η denotes the constant decay rate parameter, which usually is small. The time-surface visualizes the history of moving brightness change at each pixel location, which usually presents the edges of the scenes. The pixel values in a time-surface are rescaled from $[0, 1]$ to the range $[0, 255]$ for convenient visualization and processing.

C. Visual module

In this module we follow the work of ESVO. It is mainly divided into two parts: mapping and tracking. More details can be found in [16] and we only give a brief introduction here.

1) mapping

The mapping module consists of two steps: (i) computing depth estimates of events and (ii) fusing such depth estimates into an accurate and populated depth map.

The inverse depth of events occurred before the stereo observation, which follows a camera trajectory $\mathbf{T}_{t-\delta t:t}$, is estimated by optimizing the objective function:

$$\rho^* = \arg \min_{\rho} \mathcal{C}(x, \rho, \mathcal{T}_{left}(\cdot, t), \mathcal{T}(\cdot, t), \mathbf{T}_{t-\delta t:t}) \quad (2)$$

$$\mathcal{C} \doteq \sum_{x_{1,i} \in W_1, x_{2,i} \in W_2} r_i^2(\rho) \quad (3)$$

The residual:

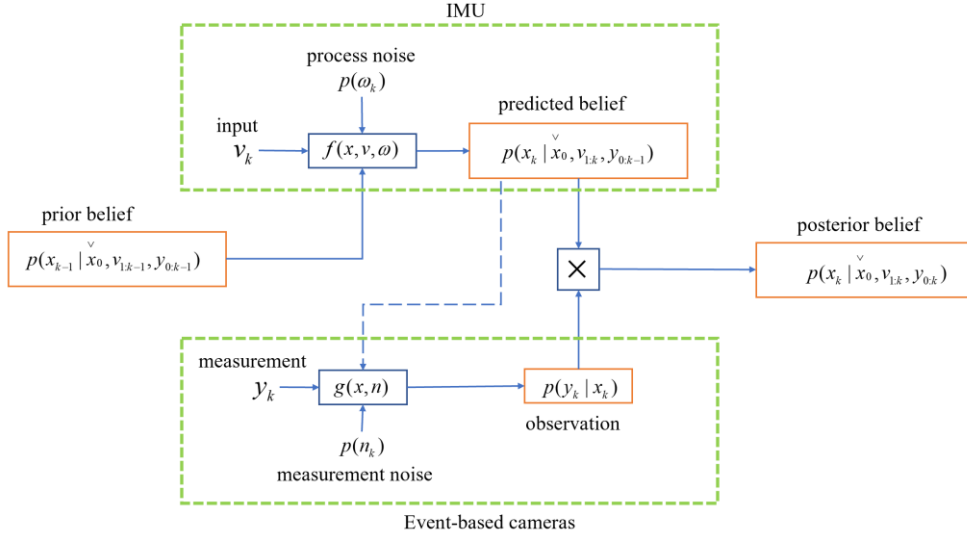


Figure 4. EKF principle

$$r_i(\rho) \doteq \mathcal{I}_{left}(x_{1,i}, t) - \mathcal{I}_{right}(x_{2,i}, t) \quad (4)$$

denotes the temporal difference between two corresponding pixels $x_{1,i}$ and $x_{2,i}$ inside neighborhoods (i.e., patches) W_1 and W_2 , centered at x_1 and x_2 respectively.

Assuming that the depth of the event point is known, each event depth estimate has a different timestamp. Then, fusing inverse depth estimates to produce a semi-dense depth map at the current time by a probabilistic approach, which is later used for tracking.

2) tracking

The problem can be formulated as follows. Let $\mathcal{S}^{\mathcal{F}_{ref}} = \{x_i\}$ be a set of pixel locations with valid inverse depth ρ_i in the reference frame \mathcal{F}_{ref} . Assuming the TS negative at time k is available, denoted by $\bar{\mathcal{I}}_{left}(\cdot, k)$, the goal is to find the pose T such that the support of the warped semi-dense map $T(\mathcal{S}^{\mathcal{F}_{ref}})$ aligns well with the minima of $\bar{\mathcal{I}}_{left}(\cdot, k)$. The overall objective of the registration is to find

$$\theta^* = \arg \min_{\theta} \sum_{x \in \mathcal{S}^{\mathcal{F}_{ref}}} (\bar{\mathcal{I}}_{left}(W(x, \rho; \theta), k))^2 \quad (5)$$

where the warping function

$$W(x, \rho; \theta) \doteq \pi_{left}(T(\pi_{ref}^{-1}(x, \rho), G(\theta))) \quad (6)$$

transfers points from \mathcal{F}_{ref} to the current frame.

D. EKF description

1) Structure of the EKF state vector

The goal of the proposed filter is to track the 3D pose of the IMU frame $\{\mathbf{I}\}$ with respect to a global frame of reference $\{\mathbf{W}\}$. An overview of the algorithm is given in Algorithm 1. The IMU measurements are processed immediately as IMU data are giving for propagating the EKF state and covariance. On the other hand, each time an observation is received, updating the state vector. The IMU state is a 15×1 vector which is defined as:

$$\mathbf{x}_{IMU} = (\mathbf{p}^T, \mathbf{v}^T, \mathbf{q}^T, \mathbf{b}_a^T, \mathbf{b}_\omega^T) \quad (7)$$

where the quaternion \mathbf{q} represents the rotation from the frame $\{\mathbf{I}\}$ to the frame $\{\mathbf{W}\}$. The vectors $\mathbf{v} \in \mathbf{R}^3$ and $\mathbf{p} \in \mathbf{R}^3$ represent the velocity and position of the body frame $\{\mathbf{I}\}$ in the world frame $\{\mathbf{W}\}$. The vectors $\mathbf{b}_a \in \mathbf{R}^3$ and $\mathbf{b}_\omega \in \mathbf{R}^3$ are the biases of the measured linear acceleration and angular velocity from the IMU, which are modeled as random walk processes, driven by the white Gaussian noise vectors $\mathbf{n}_{b\omega}$ and \mathbf{n}_{ba} , respectively. Following (7), the IMU error-state is defined as:

$$\delta \mathbf{x}_{IMU} = (\delta \mathbf{p}^T, \delta \mathbf{v}^T, \delta \mathbf{q}^T, \delta \mathbf{b}_a^T, \delta \mathbf{b}_\omega^T) \quad (8)$$

the standard additive error definition is used for the position, velocity, and biases (e.g., $\delta \mathbf{p} = \tilde{\mathbf{p}} - \mathbf{p}$, $\tilde{\mathbf{p}}$ is the real value of position and \mathbf{p} is ideal value). For the quaternion, a different error definition is employed, which is defined by the relation $\tilde{\mathbf{q}} = \mathbf{q} \otimes \delta \mathbf{q}$. The symbol \otimes denotes quaternion multiplication. The error quaternion is:

$$\delta \mathbf{q} = \begin{bmatrix} 1 \\ \delta \boldsymbol{\theta} \\ 2 \end{bmatrix} \quad (9)$$

where $\delta \boldsymbol{\theta}$ represents a small angle rotation.

2) Process model

The continuous dynamics of the IMU error-state is:

$$\begin{aligned} \delta \dot{\mathbf{p}} &= \delta \mathbf{v} \\ \delta \dot{\mathbf{v}} &= -\mathbf{R}_t [\mathbf{a}_t - \mathbf{b}_{a_t}]_{\times} \delta \boldsymbol{\theta} + \mathbf{R}_t (\mathbf{n}_a - \delta \mathbf{b}_a) \\ \delta \dot{\boldsymbol{\theta}} &= -[\boldsymbol{\omega}_t - \mathbf{b}_{\omega_t}]_{\times} \delta \boldsymbol{\theta} + \mathbf{n}_\omega - \delta \mathbf{b}_\omega \\ \delta \dot{\mathbf{b}}_a &= \mathbf{0}_{3 \times 1} \\ \delta \dot{\mathbf{b}}_\omega &= \mathbf{0}_{3 \times 1} \end{aligned} \quad (10)$$

In these expressions, \mathbf{a}_t and \mathbf{b}_t are acceleration and angular velocity from IMU measurements. $[\cdot]_{\times}$ means skew symmetric matrix. \mathbf{R}_t is the rotation matrix from frame $\{\mathbf{I}\}$ to frame $\{\mathbf{G}\}$, and \mathbf{n}_ω and \mathbf{n}_a are zero-mean, white Gaussian noise processes modeling the measurement noise. The linearized continuous-time model for the IMU error-state is:

$$\delta\dot{\mathbf{x}} = \mathbf{F}_t \delta\mathbf{x} + \mathbf{B}_t \mathbf{n}_Q \quad (11)$$

where $\mathbf{n}_Q = (\mathbf{n}_a^T, \mathbf{n}_\omega^T, \mathbf{n}_{b_a}^T, \mathbf{n}_{b_\omega}^T)^T$. The vectors \mathbf{n}_{b_a} and \mathbf{n}_{b_ω} are the random walk rate of the accelerometer and gyroscope measurement biases. \mathbf{F}_t and \mathbf{B}_t are shown in Appendix A.

To deal with discrete time measurement from the IMU, we apply median method integration to propagate the estimated IMU state:

$$\begin{aligned} \mathbf{q}_{\omega b_k} &= \mathbf{q}_{\omega b_{k-1}} \otimes \begin{bmatrix} \cos \frac{\phi}{2} \\ \boldsymbol{\phi} \\ \frac{\phi}{2} \sin \frac{\phi}{2} \end{bmatrix} \\ \mathbf{v}_k &= \mathbf{v}_{k-1} + \left(\frac{\mathbf{R}_{\omega b_k} \mathbf{a}_k + \mathbf{R}_{\omega b_{k-1}} \mathbf{a}_{k-1}}{2} - \mathbf{g} \right) (t_k - t_{k-1}) \\ \mathbf{p}_k &= \mathbf{p}_{k-1} + \frac{\mathbf{v}_k + \mathbf{v}_{k-1}}{2} (t_k - t_{k-1}) \end{aligned} \quad (12)$$

where $\boldsymbol{\phi} = \frac{\omega_{k-1} + \omega_k}{2} (t_k - t_{k-1})$, $\phi = \|\boldsymbol{\phi}\|$.

To discretize (11),

$$\delta\mathbf{x}_k = \mathbf{F}_{k-1} \delta\mathbf{x}_{k-1} + \mathbf{B}_{k-1} \mathbf{n}_k \quad (13)$$

where \mathbf{F}_{k-1} and \mathbf{B}_{k-1} are shown in Appendix B.

3) Measurement Model

We now introduce the measurement model employed for updating the state estimates. Generally, the observation equation is written as:

$$\mathbf{y} = \mathbf{G}_t \delta\mathbf{x} + \mathbf{C}_t \mathbf{n}_R \quad (14)$$

In this expression, \mathbf{G}_t is the measurement Jacobian matrix, and \mathbf{n}_R is measurement noise.

$$\mathbf{n}_R = (n_{\delta\bar{p}_x}, n_{\delta\bar{p}_y}, n_{\delta\bar{p}_z}, n_{\delta\bar{\theta}_x}, n_{\delta\bar{\theta}_y}, n_{\delta\bar{\theta}_z})^T \quad (15)$$

The noise term $\mathbf{C}_t \mathbf{n}_R$ must be zero-mean, white, and uncorrelated to the state error, for the EKF framework to be applied. In this application condition, the observation equation is:

$$\mathbf{y} = [\delta\bar{\mathbf{p}}^T, \delta\bar{\boldsymbol{\theta}}^T]^T \quad (16)$$

Then, \mathbf{G}_t and \mathbf{C}_t are:

$$\mathbf{G}_t = \begin{bmatrix} \mathbf{I}_3 & \mathbf{0}_{3 \times 3} & \mathbf{0}_{3 \times 3} & \mathbf{0}_{3 \times 3} & \mathbf{0}_{3 \times 3} \\ \mathbf{0}_{3 \times 3} & \mathbf{0}_{3 \times 3} & \mathbf{I}_3 & \mathbf{0}_{3 \times 3} & \mathbf{0}_{3 \times 3} \end{bmatrix} \quad (17)$$

$$\mathbf{C}_t = \begin{bmatrix} \mathbf{I}_3 & \mathbf{0}_{3 \times 3} \\ \mathbf{0}_{3 \times 3} & \mathbf{I}_3 \end{bmatrix} \quad (18)$$

Now, we get the equations of discrete EKF, which are shown in Appendix C.

4) Filter Update

In the preceding sections, we present the process model and measurement model. We now introduce in detail the update phase of the EKF. EKF principle is shown in Fig 4. A flowchart of the EKF is given in Fig 2-right and it is summarized in Algorithm 1.

Before we start the EKF process, we need to know the initial state of the system. In our implementation, we assume that the initial state of the system is static and take the average value of IMU output for a period of time to estimate the gravity direction. Then, we get the rotation from the IMU to the world. Next, initializing EKF parameters, including state

Algorithm1: ESVIO

- 1: Pose initialization.
 - 2: EKF initialization
 - 3: IMU propagation
 - 4: EKF prediction update
 - 5: **if** no observation
 - 6: posterior equals prior
 - 7: **else**
 - 8: EKF measurement update
 - 8: update posterior pose
 - 9: Clear the error-state
 - 10: **return** EKF state
-

vector $\delta\hat{\mathbf{x}}_0$, variance $\hat{\mathbf{P}}_0$, process noise \mathbf{Q} and observation noise \mathbf{R}_0 . Specific form is shown in Appendix D.

Then, we integrate the IMU output according to (12) for performing EKF prior estimate and executing the first two steps of EKF's five steps:

$$\begin{aligned} \delta\check{\mathbf{x}}_k &= \mathbf{F}_{k-1} \delta\hat{\mathbf{x}}_{k-1} + \mathbf{B}_{k-1} \mathbf{n}_k \\ \check{\mathbf{P}}_k &= \mathbf{F}_{k-1} \hat{\mathbf{P}}_{k-1} \mathbf{F}_{k-1}^T + \mathbf{B}_{k-1} \mathbf{Q}_k \mathbf{B}_{k-1}^T \end{aligned} \quad (19)$$

When there is no observation, posterior equals prior:

$$\begin{aligned} \delta\hat{\mathbf{x}}_k &= \delta\check{\mathbf{x}}_k \\ \hat{\mathbf{P}}_k &= \check{\mathbf{P}}_k \\ \hat{\mathbf{x}}_k &= \check{\mathbf{x}}_k \end{aligned} \quad (20)$$

When the mapping thread of visual module works, we consider an observation is received and execute the last three steps of EKF's five steps:

$$\begin{aligned} \mathbf{K}_k &= \check{\mathbf{P}}_k \mathbf{G}_k^T (\mathbf{G}_k \check{\mathbf{P}}_k \mathbf{G}_k^T + \mathbf{C}_k \mathbf{R}_k \mathbf{C}_k^T)^{-1} \\ \hat{\mathbf{P}}_k &= (\mathbf{I} - \mathbf{K}_k \mathbf{G}_k) \check{\mathbf{P}}_k \\ \delta\hat{\mathbf{x}}_k &= \delta\check{\mathbf{x}}_k + \mathbf{K}_k (\mathbf{y}_k - \mathbf{G}_k \delta\check{\mathbf{x}}_k) \end{aligned} \quad (21)$$

After that, we update the posterior pose and clear the state vector $\delta\hat{\mathbf{x}}_k$:

$$\begin{aligned} \hat{\mathbf{p}}_k &= \check{\mathbf{p}}_k - \delta\hat{\mathbf{p}}_k \\ \hat{\mathbf{v}}_k &= \check{\mathbf{v}}_k - \delta\hat{\mathbf{v}}_k \\ \hat{\mathbf{R}}_k &= \check{\mathbf{R}}_k (\mathbf{I} - [\delta\hat{\boldsymbol{\theta}}_k]_{\times}) \\ \hat{\mathbf{b}}_{ak} &= \check{\mathbf{b}}_{ak} - \delta\hat{\mathbf{b}}_{ak} \\ \hat{\mathbf{b}}_{\omega k} &= \check{\mathbf{b}}_{\omega k} - \delta\hat{\mathbf{b}}_{\omega k} \end{aligned} \quad (22)$$

The above is the whole EKF process.

IV. EXPERIMENTS

In this section, we present the datasets that we used and evaluate the proposed stereo event-based VIO system. The results show that SEVIO produces more accurate trajectories than ESVO. Some results are shown in Fig 5.

A. Datasets Used

To evaluate the proposed stereo VIO system we use sequences from publicly available datasets [38],[39]. Dataset provided by [38] was collected from a handheld rig, a flying hexacopter, a car, and a motorcycle, with calibrated sensors data from different environments. Dataset used from [39] was collected using a simple handle for hand-held, a wheeled tripod, a helmet. The scenes can be divided into two categori-

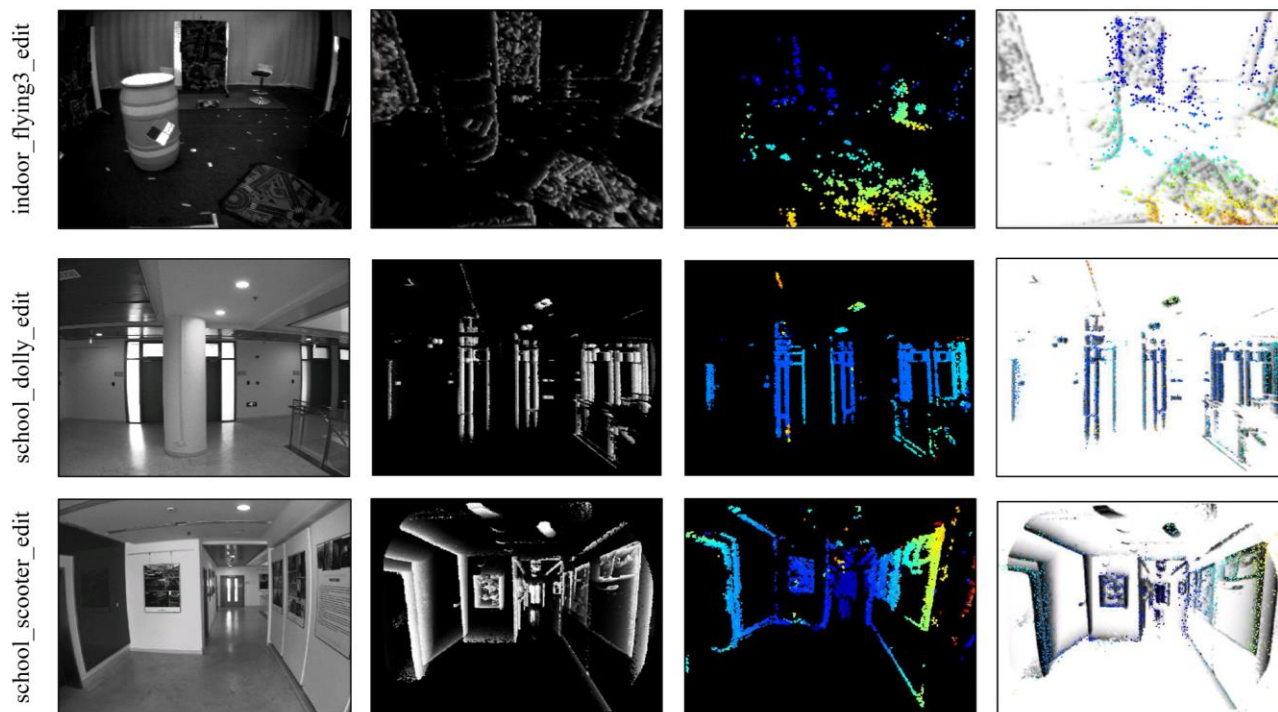


Figure 5. The first column shows images from standard camera. The second column is time surface. The third column is depth map. The last column is warping depth map overlaid on the time surface negative.

es: small-scale and large-scale.

Our algorithm works on undistorted and stereo-rectified coordinates, and cameras and imu calibration parameters are known. We used partial sequences of the above dataset to verify our algorithm. The parameters of the stereo event-camera setup in each dataset used are listed in Table I.

Table I: Parameters of various stereo event-camera rigs used in the datasets.

Dataset	Cameras	Resolutions (pixel)	Baseline (cm)
MVSEC	DAVIS 346	346×260	10.0
VEctor	Prophesee Gen3	640×480	17.0

B. Accuracy Evaluation

To show the performance of the full VIO system, we report pose estimation results by common indicators: relative pose error (RPE) and absolute pose error (APE). Since no open-source event-based VIO projects is yet available, we only compared with the stereo vision pipeline (ESVO). Because the visual module is unstable and it is difficult to main-

Table II: Absolute Pose Error and Relative Pose Error [RMSE(m)]

Sequence	ESVO		ESVIO	
	APE	RPE	APE	RPE
indoor_flying1_edit	0.190	0.014	0.299	0.011
indoor_flying3_edit	0.342	0.027	0.266	0.010
school_dolly_edit	0.990	0.077	0.703	0.075
school_scooter_edit	2.666	0.233	1.291	0.195
units_dolly_edit	0.714	0.096	0.514	0.084

tain long time working. To ensure that the trajectory is effective, we select the first part of the sequences for calculation and analysis.

The evaluation is performed on five sequences with ground truth trajectories and the evaluation results are shown in Table II. The better results per sequence are highlighted in bold. Most of the pose accuracy has been improved. Our method is less accurate than ESVO on indoor_flying1_edit. This is because after the initialization of IMU, vision still takes a period of time to initialize, resulting in obvious drift of IMU parameters. In addition, better visual parameters and filtering parameters may further improve the accuracy of the sequences.

V. CONCLUSION

In this paper, we presented an event-based stereo visual-inertial pipeline using a EKF framework. To the best of our knowledge, this is the first published work that solve this problem. Compared with the vision odometry for stereo event-based camera (ESVO [16]), our method has higher accuracy. This algorithm runs in real-time on a standard CPU and has been open sourced. In the future, there is still room for improvement in this work. The visual module is not stable to work for a long time, so vision module needs further improvement. Besides, the result with higher accuracy may be obtained by using fusion strategy based on optimization. At the same time, it will lead to higher computational power consumption. Finding a balance between accuracy and computational power consumption is also significant.

APPENDIX

APPENDIX A

The F_t and B_t in (11) are,

$$F_t = \begin{bmatrix} \mathbf{0}_{3 \times 3} & I_3 & \mathbf{0}_{3 \times 3} & \mathbf{0}_{3 \times 3} & \mathbf{0}_{3 \times 3} \\ \mathbf{0}_{3 \times 3} & \mathbf{0}_{3 \times 3} & -R_t[\mathbf{a}_t - \mathbf{b}_{a_t}]_x & -R_t & \mathbf{0}_{3 \times 3} \\ \mathbf{0}_{3 \times 3} & \mathbf{0}_{3 \times 3} & -[\boldsymbol{\omega}_t - \mathbf{b}_{\omega_t}]_x & \mathbf{0}_{3 \times 3} & -I_3 \\ \mathbf{0}_{3 \times 3} & \mathbf{0}_{3 \times 3} & \mathbf{0}_{3 \times 3} & \mathbf{0}_{3 \times 3} & \mathbf{0}_{3 \times 3} \\ \mathbf{0}_{3 \times 3} & \mathbf{0}_{3 \times 3} & \mathbf{0}_{3 \times 3} & \mathbf{0}_{3 \times 3} & \mathbf{0}_{3 \times 3} \end{bmatrix}$$

$$B_t = \begin{bmatrix} \mathbf{0}_{3 \times 3} & \mathbf{0}_{3 \times 3} & \mathbf{0}_{3 \times 3} & \mathbf{0}_{3 \times 3} \\ R_t & \mathbf{0}_{3 \times 3} & \mathbf{0}_{3 \times 3} & \mathbf{0}_{3 \times 3} \\ \mathbf{0}_{3 \times 3} & I_3 & \mathbf{0}_{3 \times 3} & \mathbf{0}_{3 \times 3} \\ \mathbf{0}_{3 \times 3} & \mathbf{0}_{3 \times 3} & I_3 & \mathbf{0}_{3 \times 3} \\ \mathbf{0}_{3 \times 3} & \mathbf{0}_{3 \times 3} & \mathbf{0}_{3 \times 3} & I_3 \end{bmatrix}$$

APPENDIX B

The F_{k-1} and B_{k-1} in (13) are,

$$F_{k-1} = I_{15} + F_t T$$

$$B_{k-1} = \begin{bmatrix} \mathbf{0}_{3 \times 3} & \mathbf{0}_{3 \times 3} & \mathbf{0}_{3 \times 3} & \mathbf{0}_{3 \times 3} \\ R_{k-1} T & \mathbf{0}_{3 \times 3} & \mathbf{0}_{3 \times 3} & \mathbf{0}_{3 \times 3} \\ \mathbf{0}_{3 \times 3} & I_3 T & \mathbf{0}_{3 \times 3} & \mathbf{0}_{3 \times 3} \\ \mathbf{0}_{3 \times 3} & \mathbf{0}_{3 \times 3} & I_3 \sqrt{T} & \mathbf{0}_{3 \times 3} \\ \mathbf{0}_{3 \times 3} & \mathbf{0}_{3 \times 3} & \mathbf{0}_{3 \times 3} & I_3 \sqrt{T} \end{bmatrix}$$

T is the period of the EKF.

APPENDIX C

Discrete EKF equation:

$$\begin{aligned} \delta \hat{\mathbf{x}}_k &= F_{k-1} \delta \hat{\mathbf{x}}_{k-1} + B_{k-1} \mathbf{n}_k \\ \hat{P}_k &= F_{k-1} \hat{P}_{k-1} F_{k-1}^T + B_{k-1} Q_k B_{k-1}^T \\ K_k &= \hat{P}_k G_k^T (G_k \hat{P}_k G_k^T + C_k R_k C_k^T)^{-1} \\ \hat{P}_k &= (I - K_k G_k) \hat{P}_k \\ \delta \hat{\mathbf{x}}_k &= \delta \hat{\mathbf{x}}_k + K_k (\mathbf{y}_k - G_k \delta \hat{\mathbf{x}}_k) \end{aligned}$$

APPENDIX D

State vector:

$$\delta \hat{\mathbf{x}}_0 = \mathbf{0}$$

Variance:

$$\hat{P}_0 = \begin{bmatrix} P_{\delta p} & \mathbf{0}_{3 \times 3} & \mathbf{0}_{3 \times 3} & \mathbf{0}_{3 \times 3} & \mathbf{0}_{3 \times 3} \\ \mathbf{0}_{3 \times 3} & P_{\delta v} & \mathbf{0}_{3 \times 3} & \mathbf{0}_{3 \times 3} & \mathbf{0}_{3 \times 3} \\ \mathbf{0}_{3 \times 3} & \mathbf{0}_{3 \times 3} & P_{\delta \theta} & \mathbf{0}_{3 \times 3} & \mathbf{0}_{3 \times 3} \\ \mathbf{0}_{3 \times 3} & \mathbf{0}_{3 \times 3} & \mathbf{0}_{3 \times 3} & P_{\delta b_a} & \mathbf{0}_{3 \times 3} \\ \mathbf{0}_{3 \times 3} & \mathbf{0}_{3 \times 3} & \mathbf{0}_{3 \times 3} & \mathbf{0}_{3 \times 3} & P_{\delta b_\omega} \end{bmatrix}$$

Process noise and observation noise:

$$Q = \begin{bmatrix} Q_a & \mathbf{0}_{3 \times 3} & \mathbf{0}_{3 \times 3} & \mathbf{0}_{3 \times 3} \\ \mathbf{0}_{3 \times 3} & Q_\omega & \mathbf{0}_{3 \times 3} & \mathbf{0}_{3 \times 3} \\ \mathbf{0}_{3 \times 3} & \mathbf{0}_{3 \times 3} & Q_{b_a} & \mathbf{0}_{3 \times 3} \\ \mathbf{0}_{3 \times 3} & \mathbf{0}_{3 \times 3} & \mathbf{0}_{3 \times 3} & Q_{b_\omega} \end{bmatrix}$$

$$R_0 = \begin{bmatrix} R_{\delta p} & \mathbf{0}_{3 \times 3} \\ \mathbf{0}_{3 \times 3} & R_{\delta \theta} \end{bmatrix}$$

REFERENCES

- [1] J. Fuentes-Pacheco, J. Ruiz-Ascencio, and J. M. Rendón-Mancha, "Visual simultaneous localization and mapping: a survey," *Artificial intelligence review*, vol. 43, no. 1, pp. 55–81, 2015.
- [2] C. Cadena, L. Carlone, H. Carrillo, Y. Latif, D. Scaramuzza, J. Neira, I. Reid, and J. J. Leonard, "Past, present, and future of simultaneous localization and mapping: Toward the robust-perception age," *IEEE Transactions on robotics*, vol. 32, no. 6, pp. 1309–1332, 2016.
- [3] P. Lichtsteiner, C. Posch, and T. Delbruck, "A 128×128 120 dB 15 μs latency asynchronous temporal contrast vision sensor," *IEEE J. Solid-State Circuits*, vol. 43, no. 2, pp. 566–576, 2008.
- [4] G. Gallego, T. Delbruck, G. Orchard, C. Bartolozzi, B. Taba, A. Censi, S. Leutenegger, A. Davison, J. Conradt, K. Daniilidis, and D. Scaramuzza, "Event-based vision: A survey," *IEEE Trans. Pattern Anal. Mach. Intell.*, 2020.
- [5] C. Brandli, R. Berner, M. Yang, S.-C. Liu, and T. Delbruck, "A 240x180 130dB 3us latency global shutter spatiotemporal vision sensor," *IEEE J. Solid-State Circuits*, vol. 49, no. 10, pp. 2333–2341, 2014.
- [6] C. Posch, D. Matolin, and R. Wohlgenannt, "A QVGA 143 dB dynamic range frame-free PWM image sensor with lossless pixel-level video compression and time-domain CDS," *IEEE J. Solid-State Circuits*, vol. 46, no. 1, pp. 259–275, Jan. 2011.
- [7] X. Lagorce, C. Meyer, S.-H. Ieng, D. Filliat, and R. Benosman, "Asynchronous event-based multikernel algorithm for high-speed visual features tracking," *IEEE Trans. Neural Netw. Learn. Syst.*, vol. 26, no. 8, pp. 1710–1720, Aug. 2015.
- [8] A. Z. Zhu, N. Atanasov, and K. Daniilidis, "Event-based feature tracking with probabilistic data association," in *IEEE Int. Conf. Robot. Autom. (ICRA)*, 2017, pp. 4465–4470.
- [9] D. Gehrig, H. Rebecq, G. Gallego, and D. Scaramuzza, "EKLT: Asynchronous photometric feature tracking using events and frames," *Int. J. Comput. Vis.*, vol. 128, pp. 601–618, 2020.
- [10] M. Cook, L. Gugelmann, F. Jug, C. Krautz, and A. Steger, "Interacting maps for fast visual interpretation," in *Int. Joint Conf. Neural Netw. (IJCNN)*, 2011, pp. 770–776.
- [11] H. Kim, A. Handa, R. Benosman, S.-H. Ieng, and A. J. Davison, "Simultaneous mosaicing and tracking with an event camera," in *British Mach. Vis. Conf. (BMVC)*, 2014.
- [12] C. Reinbacher, G. Munda, and T. Pock, "Real-time panoramic tracking for event cameras," in *IEEE Int. Conf. Comput. Photography (ICCP)*, 2017, pp. 1–9.
- [13] G. Gallego and D. Scaramuzza, "Accurate angular velocity estimation with an event camera," *IEEE Robot. Autom. Lett.*, vol. 2, no. 2, pp. 632–639, 2017.
- [14] H. Kim, S. Leutenegger, and A. J. Davison, "Real-time 3D reconstruction and 6-DoF tracking with an event camera," in *Eur. Conf. Comput. Vis. (ECCV)*, 2016.
- [15] H. Rebecq, T. Horstschäfer, G. Gallego, and D. Scaramuzza, "EVO: A geometric approach to event-based 6-DOF parallel tracking and mapping in real-time," *IEEE Robot. Autom. Lett.*, vol. 2, no. 2, pp. 593–600, 2017.
- [16] Zhou Y, Gallego G, Shen S. Event-based stereo visual odometry[J]. *IEEE Transactions on Robotics*, 2021, 37(5): 1433-1450.
- [17] H. Rebecq, G. Gallego, E. Mueggler, and D. Scaramuzza, "EMVS: Event-based multi-view stereo—3D reconstruction with an event camera in real-time," *Int. J. Comput. Vis.*, vol. 126, no. 12, pp. 1394–1414, 2018.
- [18] H. Kim, S. Leutenegger, and A. J. Davison, "Real-time 3D reconstruction and 6-DoF tracking with an event camera," in *Eur. Conf. Comput. Vis. (ECCV)*, 2016.
- [19] G. Gallego, H. Rebecq, and D. Scaramuzza, "A unifying contrast maximization framework for event cameras, with applications to motion, depth, and optical flow estimation," in *IEEE Conf. Comput. Vis. Pattern Recog. (CVPR)*, 2018.
- [20] R. Hartley and A. Zisserman, *Multiple View Geometry in Computer Vision*. Cambridge University Press, 2003, 2nd Edition.
- [21] J. Kogler, C. Sulzbachner, M. Humenberger, and F. Eibensteiner, "Address-event based stereo vision with bio-inspired silicon retina imagers," in *Advances in Theory and Applications of Stereo Vision. InTech*, 2011, pp. 165–188.

- [22] S. Schraml, A. N. Belbachir, N. Milosevic, and P. Schön, “Dynamic stereo vision system for real-time tracking,” in *IEEE Int. Symp. Circuits Syst. (ISCAS)*, 2010, pp. 1409–1412.
- [23] S.-H. Ieng, J. Carneiro, M. Osswald, and R. Benosman, “Neuromorphic event-based generalized time-based stereovision,” *Front. Neurosci.*, vol. 12, p. 442, 2018.
- [24] Y. Zhou, G. Gallego, H. Rebecq, L. Kneip, H. Li, and D. Scaramuzza, “Semi-dense 3D reconstruction with a stereo event camera,” in *Eur. Conf. Comput. Vis. (ECCV)*, 2018, pp. 242–258.
- [25] J. Kogler, M. Humenberger, and C. Sulzbachner, “Event-based stereo matching approaches for frameless address event stereo data,” in *Int. Symp. Adv. Vis. Comput. (ISVC)*, 2011, pp. 674–685.
- [26] J. Lee, T. Delbruck, P. K. J. Park, M. Pfeiffer, C.-W. Shin, H. Ryu, and B. C. Kang, “Live demonstration: Gesture-based remote control using stereo pair of dynamic vision sensors,” in *IEEE Int. Symp. Circuits Syst. (ISCAS)*, 2012.
- [27] D. Weikersdorfer, R. Hoffmann, and J. Conradt, “Simultaneous localization and mapping for event-based vision systems,” in *Int. Conf. Comput. Vis. Syst. (ICVS)*, 2013.
- [28] H. Rebecq, T. Horstschäfer, G. Gallego, and D. Scaramuzza, “EVO: A geometric approach to event-based 6-DOF parallel tracking and mapping in real-time,” *IEEE Robot. Autom. Lett.*, vol. 2, no. 2, pp. 593–600, 2017.
- [29] Zihao Zhu A, Atanasov N, Daniilidis K. Event-based visual inertial odometry[C]//Proceedings of the IEEE Conference on Computer Vision and Pattern Recognition. 2017: 5391-5399.
- [30] H. Rebecq, T. Horstschäfer, and D. Scaramuzza, “Real-time visual-inertial odometry for event cameras using keyframe-based nonlinear optimization,” in *British Mach. Vis. Conf. (BMVC)*, 2017.
- [31] E. Mueggler, G. Gallego, H. Rebecq, and D. Scaramuzza, “Continuous-time visual-inertial odometry for event cameras,” *IEEE Trans. Robot.*, vol. 34, no. 6, pp. 1425–1440, Dec. 2018.
- [32] H. Hirschmüller, “Stereo processing by semiglobal matching and mutual information,” *IEEE Trans. Pattern Anal. Mach. Intell.*, vol. 30, no. 2, pp. 328–341, Feb. 2008.
- [33] Sun K, Mohta K, Pfommer B, et al. Robust stereo visual inertial odometry for fast autonomous flight[J]. *IEEE Robotics and Automation Letters*, 2018, 3(2): 965-972.
- [34] Geneva P, Eckenhoff K, Lee W, et al. Openvins: A research platform for visual-inertial estimation[C]//2020 IEEE International Conference on Robotics and Automation (ICRA). IEEE, 2020: 4666-4672.
- [35] S.-C. Liu and T. Delbruck, “Neuromorphic sensory systems,” *Current Opinion in Neurobiology*, vol. 20, no. 3, pp. 288–295, 2010.
- [36] T. Delbruck, “Frame-free dynamic digital vision,” in *Proc. Int. Symp. Secure-Life Electron.*, 2008, pp. 21–26.
- [37] X. Lagorce, G. Orchard, F. Gallupi, B. E. Shi, and R. Benosman, “HOTS: A hierarchy of event-based time-surfaces for pattern recognition,” *IEEE Trans. Pattern Anal. Mach. Intell.*, vol. 39, no. 7, pp. 1346–1359, 2017.
- [38] Zhu A Z, Thakur D, Özaslan T, et al. The multivehicle stereo event camera dataset: An event camera dataset for 3D perception[J]. *IEEE Robotics and Automation Letters*, 2018, 3(3): 2032-2039.
- [39] Gao L, Liang Y, Yang J, et al. VECtor: A Versatile Event-Centric Benchmark for Multi-Sensor SLAM[J]. *IEEE Robotics and Automation Letters*, 2022, 7(3): 8217-8224.